
# Experimental observation of the effect of aftercavity interaction in a depressed collector gyrotron oscillator

E. M. Choi, M. A. Shapiro, J. R. Sirigiri, and R. J. Temkin

Citation: Physics of Plasmas (1994-present) **14**, 093302 (2007); doi: 10.1063/1.2776911

View online: http://dx.doi.org/10.1063/1.2776911

View Table of Contents: http://scitation.aip.org/content/aip/journal/pop/14/9?ver=pdfcov

Published by the AIP Publishing



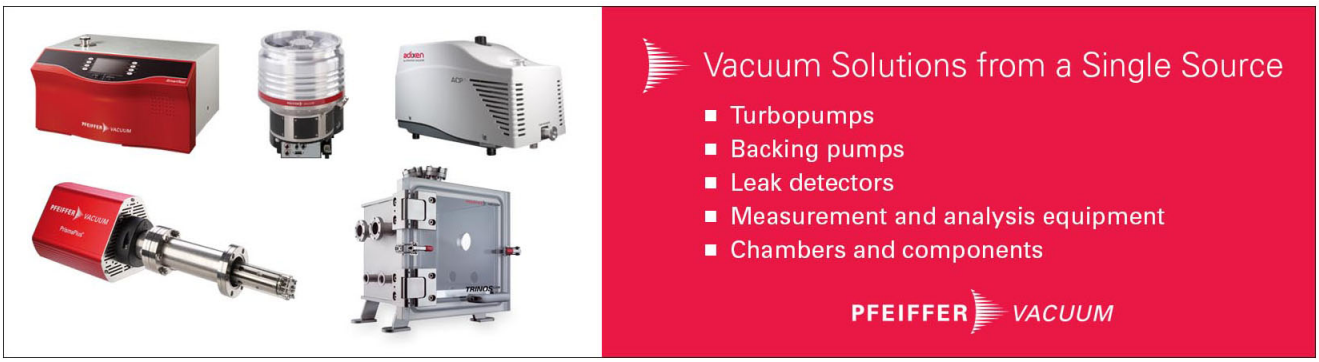

# Experimental observation of the effect of aftercavity interaction in a depressed collector gyrotron oscillator

E. M. Choi, M. A. Shapiro, J. R. Sirigiri, and R. J. Temkin
*Plasma Science and Fusion Center, Massachusetts Institute of Technology, 167 Albany Street, Cambridge, Massachusetts 02139, USA*

(Received 27 July 2007; accepted 3 August 2007; published online 27 September 2007)

This paper presents the experimental observation of the effect of an aftercavity interaction (ACI) in a depressed collector gyrotron oscillator. The gyrotron generates an output power of 1.5 MW at 110 GHz in 3 $\mu$s pulses with a 96 kV and 40 A electron beam and has a single-stage depressed collector. The ACI arises from an unintended cyclotron resonant interaction between the microwave beam traveling out from the cavity and the gyrating electron beam. The interaction occurs in the uptaper of the launcher, immediately downstream from the cavity, where the magnetic field is slightly lower than its value in the cavity region. The ACI results in a reduction in efficiency since the electron beam tends to extract power from the wave. There is also a broadening of the spent beam energy profile, which reduces the effectiveness of the depressed collector and in turn limits the overall efficiency of a gyrotron. Measurements of the maximum depression voltage of the collector vs beam current at 96 kV are compared with simulations from the MAGY code [M. Botton *et al.*, IEEE Trans. Plasma Sci. **26**, 882 (1998)]. Excellent agreement is obtained between theory and experiment but only if the ACI is included. In the present experiment, it is estimated that the observed efficiency of 50% would have been about 60% in the absence of the ACI. These results verify the role of the ACI in reducing the efficiency of the gyrotron interaction. © *2007 American Institute of Physics*. [DOI: 10.1063/1.2776911]

## I. INTRODUCTION

Gyrotrons convert rotational energy of electrons to microwave energy. This intrinsically limits the gyrotron overall efficiency because the parallel energy of electrons is not depleted in the interaction mechanism. A depressed collector recovers the unused parallel kinetic energy of electrons by means of a retarding potential in the collector with respect to the main body, so that the spent electron beam can be decelerated. Thus, depressed collectors allow a major efficiency enhancement in gyrotrons.[1,2] In theory, multistage depressed collectors are possible, but have not yet been demonstrated experimentally in gyrotrons.[3–5] Depressed collectors cannot only enhance the overall efficiency greatly but also reduce the power loading on the collector, which facilitates long-pulse operation of gyrotrons and reduces the possibility of collector failure due to metal fatigue. By reducing the voltage on the collector with respect to the body, the electrons are decelerated and the deposited thermal energy on the collector is also reduced. The depressed collector scheme has been extensively studied in conventional microwave tubes, however, there are relatively few comprehensive studies of depressed collectors in gyrotrons.

The total efficiency relationship of the gyrotron with a depressed collector can be expressed by

$$\eta_{\text{total}} = \frac{P_{\text{rf}}}{P_{\text{beam}} - P_{\text{recover}}} = \frac{\eta_{\text{imc}}\eta_{\text{int}}}{1 - \eta_{\text{coll}}(1 - \eta_{\text{int}})}, \tag{1}$$

where $\eta_{\text{int}}$, $\eta_{\text{imc}}$, and $\eta_{\text{coll}}$ designate the interaction efficiency, the internal mode converter efficiency, and the collector efficiency, respectively, and $P_{\text{rf}}$, $P_{\text{beam}}$, and $P_{\text{recover}}$ represent the generated rf power, beam power, and recovered power, respectively. $\eta_{\text{int}}$, $\eta_{\text{imc}}$, and $\eta_{\text{coll}}$ can be expressed as $P_{\text{rf}}/P_{\text{beam}}$, $P_{\text{out}}/P_{\text{rf}}$, and $P_{\text{recover}}/(P_{\text{beam}}-P_{\text{rf}})$, respectively, where $P_{\text{out}}$ is the rf output power which includes the internal rf power losses.

Figure 1 is a plot of the efficiency relationship. The overall efficiency is plotted as a function of interaction efficiency and collector efficiency. At a fixed interaction efficiency, an increase of ten percentage points in collector efficiency leads to almost five percentage points enhancement in the overall efficiency. Therefore the depressed collector can greatly increase the overall efficiency.

The efficiency of a single-stage depressed collector is strongly dependent on the energy distribution of the spent beam after the interaction in the cavity. In a single-stage depressed collector, the depression voltage of the collector is passively determined from the energy distribution of the spent beam. However, multistage depressed collectors can actively control the depression voltages at each stage by sorting the spent beam at each of the collector plates.

The collector can be depressed until the onset of body current which occurs when some of the electrons are reflected back towards the cavity. The maximum depression voltage, $V_{\text{dep}}$, that can be applied is approximately equal to the minimum energy of the spent beam. The power that is recovered by a single-stage depressed collector is $V_{\text{dep}}I_{\text{coll}}$, where $I_{\text{coll}}$ is the collector current.

Recently it has been reported by Zapevalov *et al.* that the interaction between a beam and a wave can occur at the region after a cavity, which they designated the "aftercavity interaction."[6,7] Generally, the interaction of an electron beam

 

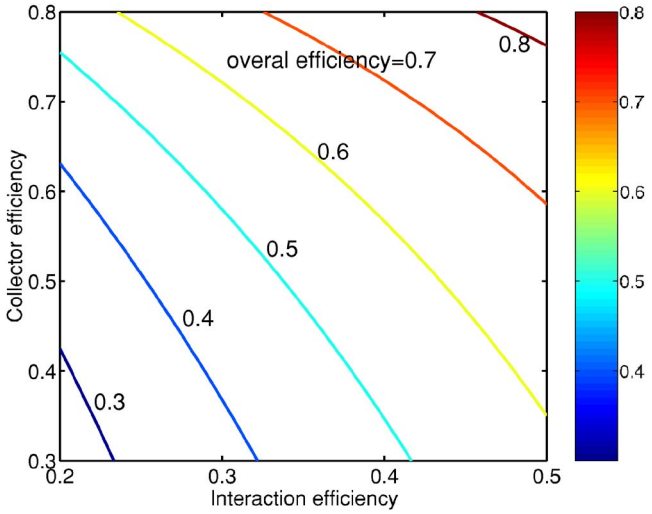


FIG. 1. (Color online) Efficiency relationship plot.

with a wave (a certain waveguide mode) takes place in the region of a cavity where the oscillation frequency $\omega$ is close to the cutoff frequency of the waveguide. In the region after the cavity, the wave becomes a traveling wave and the interaction stops. Therefore, in most gyrotrons, the efficiency does not change after the electrons pass through the cavity. However, there may be an interaction between the traveling wave and the spent electron beam after the cavity region if the output transition has a small taper, as is the case in most high power gyrotrons with an internal mode converter system. The interaction that occurs after the cavity can be a serious problem causing efficiency degradation for two reasons. First, due to the aftercavity interaction (ACI), some of the energy of the wave is reabsorbed by the electron beam. Secondly, the ACI broadens the energy spectrum of the spent beam, which results in a reduction of the maximum depression voltage that can be applied at the collector, thus limiting the energy recovery process by the depressed collector. Zapevalov *et al.* predicted that in their 170 GHz gyrotron operating in a $TE_{25,10}$ mode the reduction in efficiency due to the ACI can be 8–10 percentage points.[6]

The analytic estimation for the condition of synchronism between the rf wave and the electron beam can be calculated from the following equation:[6]

$$\omega - n\Omega_c \approx k_z v_z, \tag{2}$$

where $\omega$ is the wave frequency, $\Omega_c$ is the electron cyclotron frequency, $n$ is the harmonic number, $k_z$ is the axial wavenumber of the wave, and $v_z$ is the axial electron velocity. The interaction efficiency can be expressed as

$$\eta_{\text{int}} = \frac{\gamma_0 - \gamma_f}{\gamma_0 - 1}, \tag{3}$$

where $\gamma_0$, the initial Lorentz factor of electrons, is $1 + V_k(\text{keV})/511(\text{keV})$ and $\gamma_f$, the final Lorentz factor of the spent beam, is $(1-\beta_f^2)^{-1/2}$ where $\beta_f$ is $v_f/c$. With a given initial $\alpha_0$ and $\beta_{z0}$, $\beta_{\perp 0}$ can be obtained from $\alpha_0 = \beta_{\perp 0}/\beta_{z0}$ where $\beta = v/c$. $\beta_{\perp f}$ is now calculated from $\beta_f$. Therefore, after the interaction in the cavity between the electron beam and the wave, the perpendicular and parallel velocities of the spent beam are expressed in accordance with the adiabatic invariant as follows:

$$\beta_\perp = \beta_{\perp f}\sqrt{\frac{B(z)}{B_{0,\max}}}, \quad \beta_z = \sqrt{\beta^2 - \beta_\perp^2}, \tag{4}$$

where $B(z)$ is the tapered magnetic field and $B_{0,\max}$ is the maximum magnetic field which occurs at the center of the cavity. The cyclotron frequency, $\Omega_c$, can now be expressed for a tapered magnetic field and geometry as

$$\Omega_c = (\omega - \Delta\Omega_c)\left(\frac{\gamma_0}{\gamma_f}\right)\left(\frac{B(z)}{B_{0,\max}}\right) \tag{5}$$

using $\Omega = \Omega_0(\gamma_0/\gamma_f)(B(z)/B_{0,\max})$ and $\Omega_0 = \Omega - \Delta\Omega_c$. Using Eqs. (4) and (5), the cyclotron resonance condition, Eq. (2), is written as

$$1 - \left(1 - \frac{\Delta\Omega_c}{\omega}\right)\left(\frac{\gamma_0}{\gamma_f}\right)\left(\frac{B(z)}{B_{0,\max}}\right) = \beta_z\left(1 - \left(\frac{r_c}{r(z)}\right)^2\right)^{1/2}, \tag{6}$$

where $r_c$ is the cavity radius and $r(z)$ defines the geometry of the section downstream from the cavity.

## II. EXPERIMENTAL RESULTS

Figure 2 is the schematic of the experimental gyrotron with a single-stage depressed collector. The magnetron injection gun (MIG), which generates an electron beam at 96 kV with a beam current of 40 A, has been used in previous experiments.[8] The internal mode converter consists of a launcher that transforms a $TE_{22,6}$ cavity mode into a

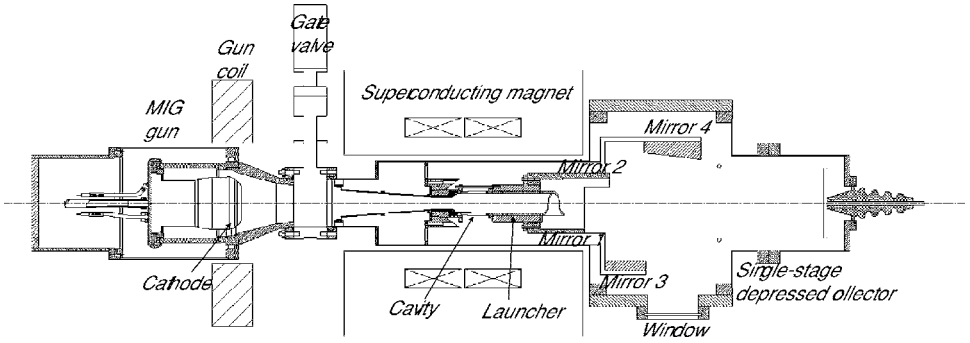


FIG. 2. Schematic of the single-stage depressed collector 1.5 MW, 110 GHz gyrotron.

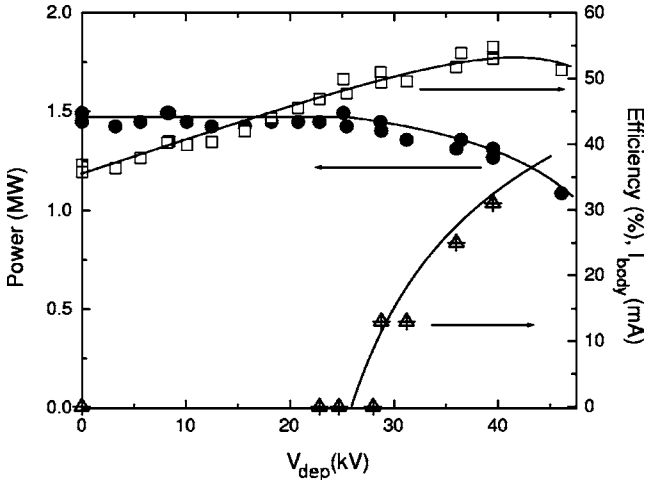


FIG. 3. Power, efficiency, and body current measurements as a function of depression voltage of the collector for operation at a voltage of 96.6 kV and a current of 42 A. Solid circles: output power; open squares: efficiency; open triangles: body current.

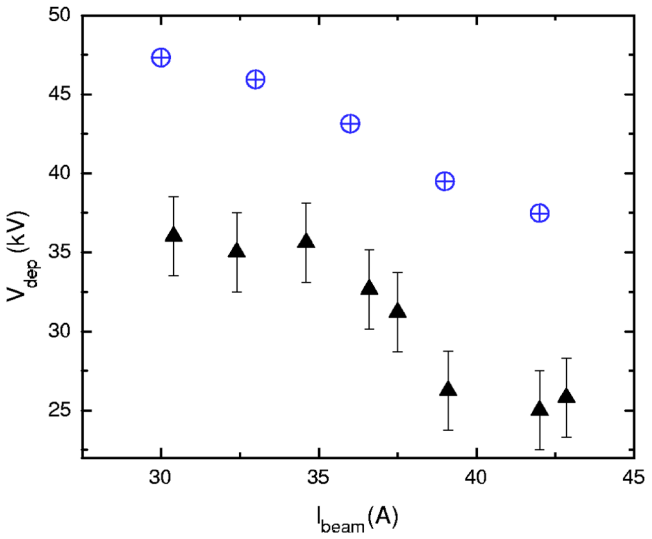


FIG. 4. (Color online) The voltage threshold of collector depression as a function of beam current at a fixed beam voltage of 96.6 kV. Triangles with error bars represent experimental measurements and crossed-circles represent the simulation results.

Gaussian-type beam and 4 mirrors that focus and guide the Gaussian-type beam to the window. The single-stage depressed collector is a copper cylinder whose diameter is 13.7 cm and length is 19.7 cm. It is isolated from the tube body by a ceramic insulating break rated up to 45 kV.

In Fig. 3, power, efficiency, and body current are plotted as a function of collector depression voltage. The output power is stable at 1.5 MW up to a depression voltage of 25 kV without an appearance of body current. The achieved efficiency at a depression voltage of 25 kV is 50%. As the depression voltage exceeds 25 kV, there is an onset of body current and the output power begins to decrease. The efficiency increases up to 55% at a depression voltage of 40 kV, but the power drops to 1.3 MW and the body current increases to 30 mA. Operation at a voltage depression above 25 kV would not be viable for a long pulse or CW gyrotron due to the finite body current interception.

The applicable critical (threshold) depression voltages ($V_{\mathrm{dep}}$) were measured as a function of beam current ($I_{\mathrm{beam}}$) at a fixed beam voltage of 96.6 kV and are shown in Fig. 4. Also shown are simulation results obtained with the MAGY code, a gyrotron and gyroklystron code widely used for designing and analyzing gyrotron cavities.[9] The simulation was done with the experimental cavity geometry and the experimental magnetic field profile. The launcher geometry after the cavity region was not included in these simulations, which means that the ACI is not included in this first analysis. The effect of the ACI will be considered later in this section. The applicable critical (threshold) depression voltages were determined by noting the onset of body current. Experimentally, a depression voltage of 25 kV could be achieved at 42 A at 96.6 kV, whereas the simulation predicts 37.5 kV. Operation with a depression voltage of 37.5 kV would raise the overall efficiency from 50% to 60%. Thus, agreement between theory and experiment without the ACI is poor.

In order to include the ACI, we first consider the location where the synchronism condition is satisfied after the cavity. The region can be calculated analytically using Eq. (6). The accelerating beam voltage is 96 kV and therefore $\gamma_0$ is 1.1879. With $\alpha_0=1.3$, $\beta_{\perp 0}$ and $\beta_{z0}$ are found to be 0.4278 and 0.3291, respectively. With the geometries of the cavity and the launcher and the tapered magnetic field shown in the first graph in Fig. 5, the location where the synchronism condition is satisfied is $z \simeq 11$ cm.

Figure 5 shows an example of a simulation of the ACI in MAGY. The mode conversion was checked for our launcher geometry by using the CASCADE code, which calculates coupled-mode equations for a given geometry.[10] CASCADE predicts that there is no significant mode conversion after the cavity region. In the ACI, the net result is that the electron beam extracts power from the wave and some electrons will be accelerated. The electric field amplitude of the $TE_{22,6}$ mode and its phase are plotted. The varying phase after the

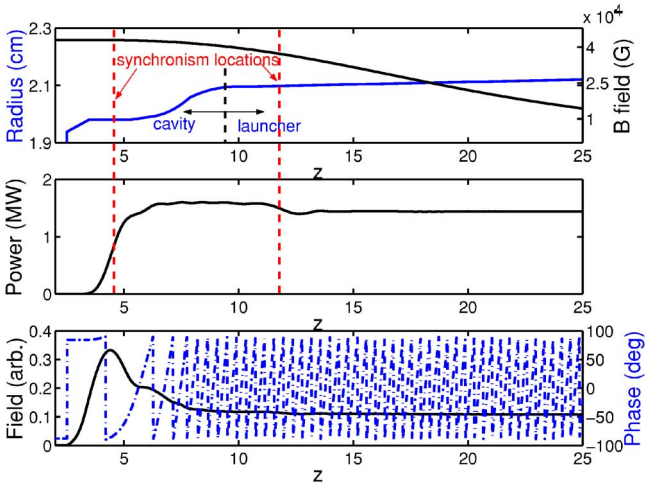


FIG. 5. (Color online) Geometry, main magnetic field, output power, longitudinal field distribution of the $TE_{22,6}$ mode and phase plots in the cavity and the launcher simulated from MAGY.

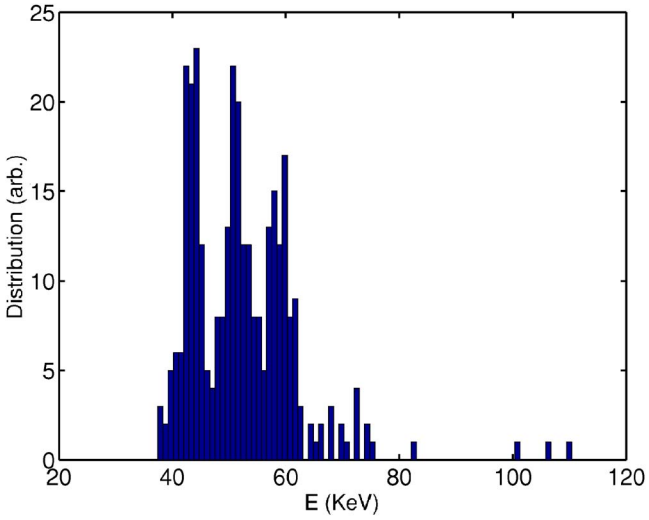


FIG. 6. (Color online) The simulated energy distribution of the spent beam from MAGY at $z=9.82$ cm (the position of the cavity end).

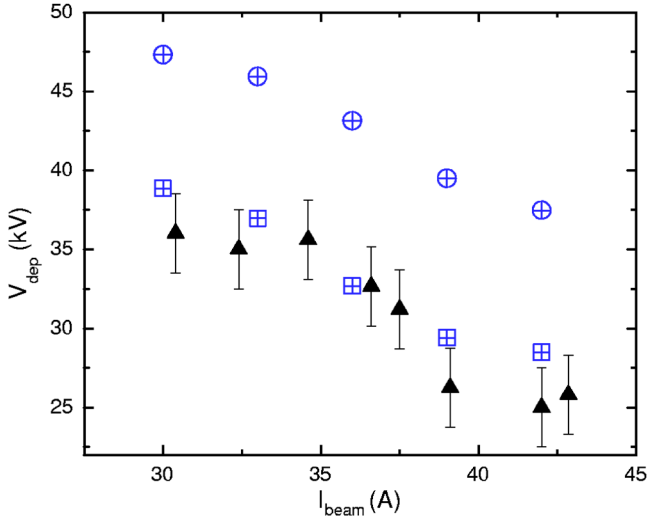


FIG. 8. (Color online) The voltage threshold of collector depression as a function of beam current at 96.6 kV beam voltage. Triangles with error bars represent experimental measurements and crossed-circles and squares represent the simulated results without the ACI and with the ACI, respectively.

cavity shows a traveling wave. The middle plot of Fig. 5 is the output power as a function of $z$. The power starts to drop at $z \simeq 11-13$ cm from 1.58 MW to 1.44 MW, corresponding to a reduction in efficiency from 39% to 36%. The location of the drop in efficiency from MAGY calculation is in agreement with the location of the synchronism condition at $z=11$ cm calculated analytically.

The resultant energy distribution of the spent electron beam without including the ACI, which means the simulation is stopped before the launcher begins, is plotted in Fig. 6. The simulations were done with 81 beamlets, at a voltage of 96 kV, with a beam current of 42 A, alpha of 1.3, velocity spread of 7%, and output power of 1.58 MW. The minimum energy of the spent beam is 37.5 keV as shown in Fig. 6, which is also plotted for comparison with the result of the experiment in Fig. 4. When the ACI is considered by including the tapered launcher, the energy distribution of the spent beam is in fact changed as shown in Fig. 7. It is broader than the distribution without the ACI and the minimum energy of the spent beam is reduced to 28.5 kV. The final results for the voltage threshold are plotted in Fig. 8 with and without inclusion of the ACI. As seen in Fig. 8, the simulation results that include the ACI, which are represented as cross-squares, show excellent agreement with the experimental results at all beam current values. This strongly indicates that the ACI is a major effect in degrading the overall efficiency.

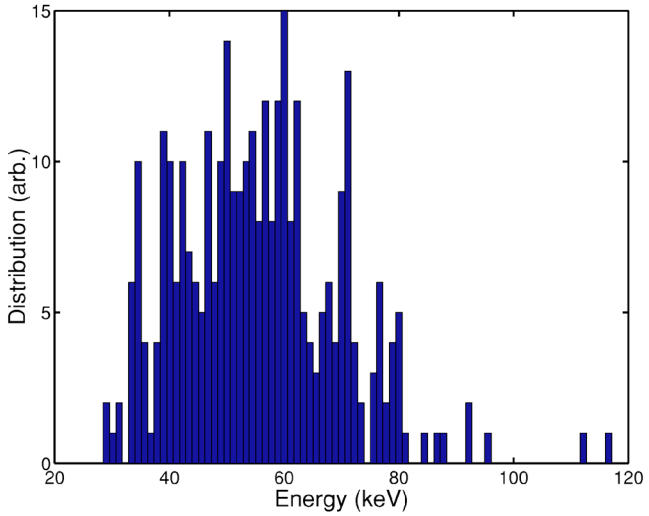


FIG. 7. (Color online) The simulated energy distribution of the spent beam from MAGY at $z=25.02$ cm (the position of the launcher end).

## III. DISCUSSION AND CONCLUSIONS

A single-stage depressed collector experiment in a 1.5 MW, 110 GHz gyrotron has been successfully performed. The maximum efficiency is 50% at an output power of 1.5 MW with a single-stage collector depressed by 25 kV. The efficiency of the single-stage depressed collector is 41%. The discrepancy between theory and experiment in terms of the critical depression voltage, which essentially is determined by the minimum energy of the spent beam, is explained by considering the aftercavity interaction (ACI). From this study, it emerges that a cavity tapered section and an internal mode converter have to be designed with great care in order to prevent the degradation of efficiency due to the ACI. In fact, if the ACI were completely avoided, an overall efficiency of about 60% could have been achieved in this experiment. The ACI between the traveling wave and the spent beam was observed in the MAGY simulation in our geometry. Since the ACI occurs in a region that is not far from the end of the cavity, it may be difficult to eliminate it in most cases. Experiments should be designed from the outset so as to produce the correct magnetic field or waveguide taper to avoid the ACI.

## ACKNOWLEDGMENTS

The authors would like to thank W. Mulligan and I. Mastovsky for their help in running the experiment and Dr. A. Vlasov for valuable discussions in MAGY simulations.

[1]K. Sakamoto, M. Tsuneoka, A. Kasugai, T. Imai, T. Kariya, K. Hayashi, and Y. Mitsunaka, Phys. Rev. Lett. **73**, 3532 (1994).
[2]B. Piosczyk, C. Iatrou, G. Dammertz, and M. Thumm, IEEE Trans. Plasma Sci. **24**, 579 (1996).
[3]A. Singh, S. Rajapatirana, Y. Men, V. L. Granatstein, R. L. Ives, and A. J. Antolak, IEEE Trans. Plasma Sci. **27**, 490 (1999).
[4]A. Singh, A. Valfells, M. J. Kolander, and V. L. Granatstein, IEEE Trans. Plasma Sci. **32**, 1267 (2004).
[5]G. Ling, B. Piosczyk, and M. K. Thumm, IEEE Trans. Plasma Sci. **28**, 606 (2000).
[6]V. E. Zapevalov and M. A. Moiseev, Radiophys. Quantum Electron. **47**, 520 (2004).
[7]N. A. Zavolsky, V. E. Zapevalov, and M. A. Moiseev, Radiophys. Quantum Electron. **49**, 108 (2006).
[8]E. M. Choi, C. D. Marchewka, M. A. Shapiro, J. R. Sirigiri, I. Mastovsky, and R. J. Temkin, Phys. Plasmas **13**, 023103 (2006).
[9]M. Botton, T. M. Antonsen Jr., B. Levush, A. Vlasov, and K. Nguyen, IEEE Trans. Plasma Sci. **26**, 882 (1998).
[10]CASCADE: Cascade engine V1.60, Calabazas Creek Research, Inc., Saratoga, CA, 2001.